

Multi-Sensor Fault Diagnosis for Misalignment and Unbalance Detection Using Machine Learning

Tauheed Mian , Anurag Choudhary , Member, IEEE, and Shahab Fatima 

Abstract—Rotating machines frequently undergo various faults causing increased maintenance and operation costs. To minimize these costs, effective and intelligent methods are thus required. Different sensor modalities reflecting various faults should continuously be monitored and interpreted to enable these methods. In this work, two sensor modalities, **Infrared Thermography (IRT)**, and **vibration** are used complementary to form a multi-sensor fault diagnosis system. This system is used to diagnose the three most occurring faults: **misalignment, unbalance, and rotor disk eccentricity**, as single, dual, and multi-faults in a rotating mechanical system. The high feature processing capabilities of a Deep Convolutional Neural Network (DCNN) and the high predictive capabilities of a Support Vector Machine (SVM) are combined along with the potential dimensionality reduction using Principal Component Analysis (PCA). The results show that the proposed method is robust and signifies its reliability towards the effective diagnosis of considered faults. Further, IRT-based fault diagnosis outperforms the vibration-based classification in all working conditions.

Index Terms—Fault diagnosis, infrared thermography, vibration monitoring, machine learning.

I. INTRODUCTION

ROTATING machines are inherent to any power generation plant and production system. It has various essential components, including prime mover, connecting shafts, pump, gear, etc., and faults in these components could lead to significant losses [1]. Rotating machines continually run for a long time in the actual industrial scenario. This situation leads to misalignment, unbalance, and sometimes rotor eccentricity problems. These pervasive problems lead to other major catastrophic losses, component damage, and sometimes vital loss [2], [3]. In such circumstances, the reliable operation of these machines is crucial for the dependent components' access to

Manuscript received 11 January 2023; revised 15 March 2023 and 9 May 2023; accepted 7 June 2023. Date of publication 16 June 2023; date of current version 20 September 2023. Paper 2023-IACC-0026.R2, presented at the 2022 IEEE International Conference on Power Electronics, Smart Grid, and Renewable Energy, Trivandrum, India, Jan. 02–05, and approved for publication in the IEEE TRANSACTIONS ON INDUSTRY APPLICATIONS by the Industrial Automation and Control Committee of the IEEE Industry Applications Society [DOI: 10.1109/PESGRE52268.2022.9715938]. (Corresponding author: Tauheed Mian.)

Tauheed Mian and Shahab Fatima are with the Centre for Automotive Research and Tribology, Indian Institute of Technology Delhi, New Delhi 110016, India (e-mail: tauheedm.iitd@gmail.com; fatima@iitd.ac.in).

Anurag Choudhary is with the School of Interdisciplinary Research, Indian Institute of Technology Delhi, New Delhi 110016, India (e-mail: anurag.choudhary087@gmail.com).

Color versions of one or more figures in this article are available at <https://doi.org/10.1109/TIA.2023.3286833>.

Digital Object Identifier 10.1109/TIA.2023.3286833

high-quality goods and services [4]. An efficient fault diagnosis system significantly reduces the cost of maintenance caused due to various component failures [5]. Shaft misalignment majorly arises due to faulty machine assembly [6]. Similarly, unbalance is induced whenever the center of mass of the rotor disk does not match its center of rotation [7]. In recent years, various methods have been explored using different modalities to diagnose these mentioned faults. Vibration monitoring is a proven technique for the diagnosis of faults in rotating machines that has been used for a long time [8]. Traditionally model-based approaches are used for diagnosing different faults using vibration sensors. It has been shown that even multiples of the fundamental frequency are significantly affected by the vibration response due to coupling misalignment [9]. The misalignment and unbalance faults were modeled and analyzed in a rotor-bearing system for flexural vibrations [10]. A unique trial misalignment approach was presented to simultaneously estimate the residual rotor misalignment and unbalance [11]. However, due to the emergence and development of data-driven approaches, model-based approaches are seldom in often practice. In general, vibration monitoring is capable to deal with the acquisition of information regarding the mechanical behavior of the machine components. This information is helpful for the analysis of mechanical faults through empirical relations [12]. However, vibration monitoring has some limitations in practical working conditions, such as contact nature, frequent calibration, and mounting issues in harsh environments [13].

Non-invasive techniques can be helpful in the diagnosis of a variety of faults in rotating machinery in order to deal with these issues. IRT is a non-invasive methodology for fault diagnosis that has gained much attention from researchers in the past two decades [14]. Over recent years, IRT technology has become a viable alternative to in-situ temperature measuring sensors such as thermocouples [15]. There are commercial IRT cameras used to measure the heat radiated from a surface. These cameras make it easy to assess the temperature observed at the surfaces from a distance [16]. According to the Hertzian contact theory, an increase in bearing preloads can also happen when the temperature changes due to thermal expansion [17]. Misalignment, unbalance, and eccentricity also impact the bearings by inducing excessive vibrations. Therefore, it is essential to identify any instances of these faults as soon as possible to prolong the operational life of the machine [18].

Preserving the inherent advantages, IRT also has some issues, such as the influence of environmental factors and the effect of reflection in case of low emissivity material. In general any single modality sensor has limitation pertaining to the incapability to measure all the states of machine. Nevertheless, technological

advancement in the present era makes industries to adopt more sophisticated and reliable diagnosis systems for machine components to survive in the ongoing competitive environment. In such cases, using information from a single sensor becomes insufficient for formulating an effective fault diagnosis system. For a reliable fault diagnosis system, two or more modality sensors can be installed [19], [20]. Using multi-modality sensors in the diagnosis system has three significant benefits: **enhanced reliability, information regarding unmeasured states, and quality data** [21]. Various rotating machine faults were investigated by analyzing vibration signals and thermal images, and this multi-sensor fault detection system was shown to perform significantly better than the modality alone [22].

In determining whether a multi-sensor system is more cost-effective than a single-sensor system or not, **the number of sensors** used is also a consideration [23]. This entails applying a multi-sensor-based diagnosis system, especially where multi-faults exist in the rotating machine system. The existence of multi-faults in rotating machines is a practical issue for the industry; hence, effective ways to diagnose them must be put into practice. **In recent decades artificial intelligence approaches, including Machine Learning (ML) and Deep Learning (DL), have gained much popularity for the diagnosis of different faults in rotating machine components** [24]. Among various available ML approaches, some popular methods are **SVM, artificial neural network, k-nearest neighbour, and random forest** [25]. Preserving various advantages, these models rely on manual feature extraction. **With the development of computational power in recent times, DL-based methods got much popularity due to their automated feature extraction capability** [26], [27]. However, when dealing with a specific feature type, ML models retain their effectiveness with low computational cost and easy implementation [28].

From the literature investigations, it has been observed that both IRT and vibration monitoring can be employed to detect and diagnose faults in rotating machinery. By looking at abnormal thermal patterns using IRT, it is possible to detect problems such as misalignment, unbalance, and other issues in rotating machines. Vibration monitoring involves measuring the machine's vibration using sensors and analyzing the data to detect various faults. Further, in a situation where more than one fault co-exists, the use of different modality sensors is the need to form a multilateral and reliable fault diagnosis system. This ensures timely and effective decision-making for the diagnosis of faults and to take of necessary actions accordingly. **To the best of the authors' knowledge, very less work is reported for the intelligent diagnosis of frequently occurring faults such as misalignment, unbalance, and rotor disk eccentricity, either considering them individually or in combination.**

Further, the IRT, along with vibration monitoring, has not been explored for these faults. Comparing the performance of IRT and vibration monitoring for detecting and diagnosing misalignment, unbalance, and eccentricity faults can provide useful insights into the strengths and limitations of these techniques. Combining these methods in a complementary manner is helpful in forming a multi-sensor diagnosis system with enhanced reliability. Following are the main contribution of the proposed work.

- Most encountered faults in rotating machinery, including misalignment, unbalance, and eccentricity, are experimentally investigated as **single, dual, and multi-faults**.

- IRT and vibration monitoring are employed to constitute a multi-sensor fault diagnosis system resulting in enhanced reliability.
- A DCNN-SVM based automated diagnosis system is adopted with robust feature processing and predictive characteristic.

The following sections make up the remaining portions of the article. The methodology for the proposed work is covered in Section II, the experimental details for data acquisition are described in Section III, the results are explained in Section IV, and the conclusion is provided in Section V.

II. PROPOSED METHODOLOGY

The present work adopted IRT and vibration monitoring to develop a reliable fault diagnosis system for different fault conditions. For IRT, thermal images are extracted from the recorded video, and further, the background of these images is removed using color thresholding. **For vibration monitoring, the data is converted to time-frequency images using Constant Q Transform (CQT) owing to its inherent advantage of the variable resolution.** The preprocessed images are then used for automated feature extraction using a DCNN. After that, PCA is used for dimensionality reduction, followed by classification using SVM. The schematic diagram of the proposed methodology is shown in Fig. 1.

A. IRT Based Image Extraction

The induced loads caused by various faults contribute to heat generation in rotating machine components. By observing the temperature rate at the couplings, induced misalignment at the shaft can be identified [29]. Similarly, unbalance and eccentricity also contribute to induced force and hence the heat generation at the bearing [30]. IRT uses the principle of heat dissipation by any surface. Each body emits some thermal energy, and this principle is helpful for fault diagnosis in rotating machines. **At a steady state, the amount of heat transported to the environment and the shaft equals amount of heat produced.** Additionally, the bearing achieves a consistent temperature in a steady state. The rate of temperature change related to the rotating components can be anticipated by a thermal analysis utilizing the fundamental equation of thermodynamics as given below that provided the total heat as:

$$Q = Q_h + Q_r + Q_k + mc \frac{\delta T}{\delta t} \quad (1)$$

Here, Q_h , Q_r , and Q_k belong to convection, radiation, and conduction heat energy, respectively. Further, m is the mass of the body, and c denotes the specific heat. T is the absolute temperature of the surface and t is time. In order to comprehend the heat transfer mechanisms, researchers have considered both the **assumption of lumped mass** in addition to the whole thermal network. **Since the bearing or coupling's Biot number is typically much below 1 and convection to the surrounding air is the primary mechanism of heat transmission, it can be thought of as a lumped parameter system** [31].

To determine the overall convective heat transfer coefficient, researchers have examined the temperature reduction rate when a system first stops. The system's **time constant** affects how quickly temperatures drop. The rate of temperature fall will be comparatively slower for systems with large time constants [32].

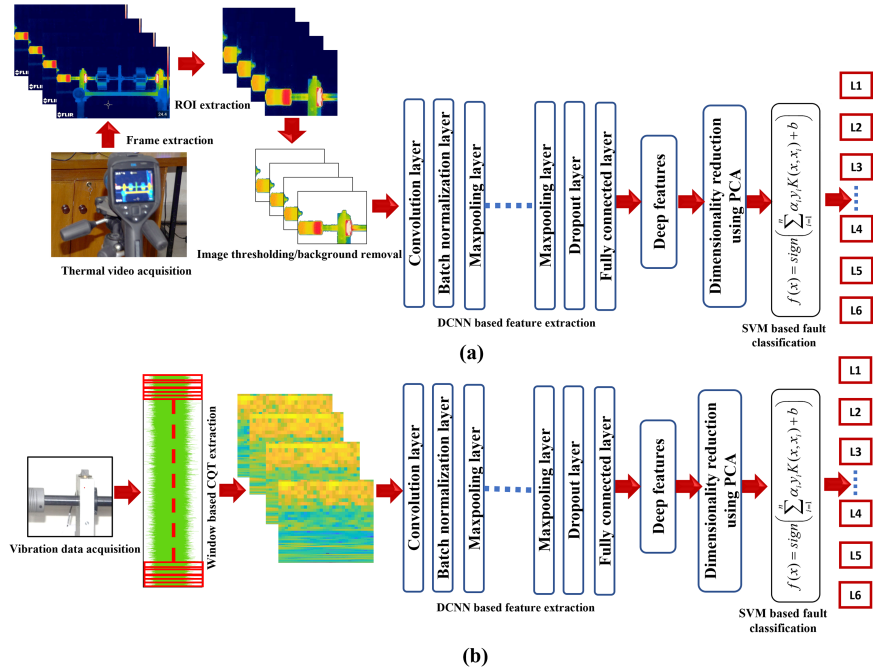


Fig. 1. Methodology for multi-sensor-based fault diagnosis: (a) IRT. (b) Vibration.

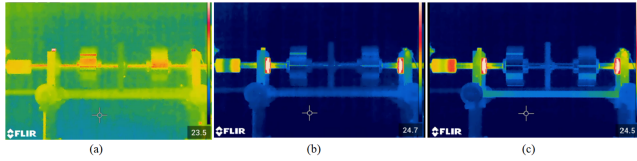


Fig. 2. IRT images at: (a) Time = 0 seconds. (b) Time = 1200 seconds. (c) Time = 1800 seconds.

Researchers have traditionally used contact-type temperature sensors for monitoring abnormalities in the machines. However, using contact-type sensors such as thermocouples to detect coupling temperatures is challenging due to continuous rotation [33]. The IRT approach is a relatively efficient and easy-to-use tool for studying thermodynamic behavior [34]. Each object radiates heat that can be characterized by Stefan Boltzmann law as given below:

$$Q_r = \varepsilon \sigma T^4 \quad (2)$$

Here, Q_r stands for total radiation energy, emissivity is given by ε , and σ is regarded as the Stefan-Boltzmann constant [35]. T is the absolute temperature of the surface. As faults develop in rotating machine components, these phenomena occur, promoting the employment of IRT as a potential fault diagnosis approach. In [18], a typical monitoring guideline is given about IRT data capturing at a steady state in consideration of the heat transfer effect to the proximity. Different fault conditions can be compared through image capturing at a steady state condition [22]. The steady-state condition is described when the temperature of the system does not significantly change with time i.e., the state of thermal equilibrium. Fig. 2(a) and Fig. 2(b) show the thermal image when the fault simulator is not running and after 1200 seconds of running, respectively. Similarly, Fig. 2(c) shows the thermal image at 1800 seconds. It can be observed from this figure that at steady state condition, the

heat distribution is much clear. Further, in the present study, misalignment is involved, making it logical to consider the coupling in the Region of Interest (RoI) as temperature rise at the coupling due to the additional torsional effects. Such thermal images can be significantly employed for accurate fault diagnosis. All the extracted thermal images contain a background that might hinder the pattern recognition task. So, the background of the thermal images is removed through color thresholding. The color threshold segments color images incorporating thresholding different color channels according to different color spaces. Using this, a binary segmentation mask is created and applied to all extracted thermal images.

B. Time-Frequency Image Extraction

The CQT is an improved wavelet transform that is useful for expressing the signal in lower frequencies, helping to resolve the issue of frequency mapping across a logarithmic scale. In the CQT, the inverse discrete Fourier transform is carried out after the Gabor frames are applied to the input signal's discrete Fourier transform [36]. Since CQT offers perceptually better representation in accordance with the human perception system, it was initially created to process music data. The signals generated from the rotating machines are also non-stationary and thus have very similar characteristics. As a result, CQT could be seen as a solid choice for identifying faults in these machines as fault features predominate in the shaft frequency. The CQT aims to achieve a time-frequency feature with a constant Q factor over the entire frequency axis by geometrically separating the filter center frequencies [37]. As a result, it may achieve a higher temporal resolution at higher frequencies and a higher frequency resolution at a lower frequency. If $x(t)$ is the discrete time signal of vibration, then CQT is given as:

$$X_{CQT}(n, k) = \sum_{j=0}^{K_n-1} x(j) \alpha_n^* \left(j - k + \frac{K_n}{2} \right) \quad (3)$$

Here, K_n is regarded as window length with n is the frequency bin. $\alpha_n^*(k)$ is basically complex conjugate of the function given as:

$$\alpha_n(k) = \frac{1}{K_n} w\left(\frac{n}{K_n}\right) e^{-j2\pi n \frac{f_n}{f_s}} \quad (4)$$

Here f_n is regarded as center frequency of n th bin with sampling frequency as f_s , and w is the window function. f_n can be given as:

$$f_n = f_1 * 2^{\frac{n-1}{P}} \quad (5)$$

Here, the center frequency for the first bin is given as f_1 , and P is bins per octave. It can be seen that the window size and center frequency values here vary with frequency values in contrast to standard Short-Time Fourier Transform (STFT). Thus, CQT produces a constant Q value as a result for all frequency settings resulting in more detailed spectral variation. A window size of 556 data points is used for the extraction of time-frequency images. An optimal overlapping of 50% is considered to minimize the chances of information loss. This results in the total time-frequency images of 6900 for each class.

C. Feature Extraction and Fault Classification

Deep CNN has an excellent ability to automatically extract features and classify data. Further, SVM is a viable contender for the classification problem because of its strong capacity to process limited samples and its strong generalization capabilities. Further, the dimensionality reduction is done using the PCA before the input to SVM to reduce the feature correlation for better and generalize training.

The main objective involved in the extraction of features is to produce multilevel and deeply rooted feature vectors. The convolutional layers at the initial part of the DCNN network learn low-level features and have a small receptive field. The inputs are convoluted using several convolution kernels or filters by the DCNN model. These filters include color filters and edge detectors. Deeper layers pick up high-level combinations of the features that the previous layers have already learned. So, the network's final layers have larger receptive fields and learn complex features. Filter for the final layers has the capability to detect much more complex patterns than the initial layers [38]. This leads to the extraction of detailed abstract and invariant features [39].

Mathematically, the convolution operation is given as:

$$p_k^j = \sum_{i \in N_j} X_i^{k-1} * W_{ij}^k + b_j^k \quad (6)$$

Here, the j th feature map's activation value in layer k , is given by X_i^{k-1} and, N_j is the number of feature maps in the layer. W_{ij}^k denote the weight matrix, b_j^k is called the bias, and $*$ denotes the convolution operation. To enhance the learning capability for efficient feature extraction, the convolution layer is assisted with the Rectified Linear unit (ReLU). Different activation functions affect the model's ability to non-linear fitting in different ways. CNNs with ReLu as an activation function more likely to be trained many times faster as compared to their equivalents having sigmoid or hyperbolic tangents as activation functions. ReLu has the significant benefit of preventing the onset of the serious issue known as vanishing gradient [40]. In the proposed structure of the DCNN batch normalization layers are also added to overcome problem of internal covariate shift. A pooling layer

seeks to combine related local characteristics. By doing this, translational invariance is preserved while reducing the dimension of feature maps and parameters. The current architecture involves four convolution and four pooling layers, along with one fully connected layer. The architecture uses input image size of $96 \times 96 \times 3$. Here, max-pooling is adopted as it has a faster convergence rate. This operation is given for the feature map C_j :

$$P_j = \max(C_j) \quad (7)$$

The last layer of DCNN is the fully connected layer. Considering the input and output vector lengths are P and Q respectively, the count of parameters in a fully connected layer is given as:

$$N = P * Q + Q \quad (8)$$

The features are extracted from the fully connected layer. To further reduce the computation cost and persevering the lucidity of the fault diagnosis system, PCA is used to reduce the dimensions of the features extracted from the fully connected layer. Eliminating irrelevant variables, it enables machine learning algorithms to analyze data more quickly and efficiently [41]. In this process, data normalization is the first step, followed by the calculation of the covariance matrix. Further, the eigenvalues of the covariance matrix and contribution rate are calculated. Finally, the ranking is done based on the contribution rate, and principal components are selected. The highest value of variance found along the first principal component indicates the least amount of information loss as discussed in [42].

The feature set with reduced dimensionality is used as input to a quadratic SVM to diagnose different single, dual, and multi-fault. The inherent advantage and potential of quadratic SVM to solve the problem of linear inseparability make it a suitable choice for the classification [43]. Here, the main objective is to find the best hyperplane to maximize the space between classes. A soft interval maximization problem can be used to characterize its learning as:

$$\min \frac{1}{2} \|w\|^2 |C \sum_{i=1}^m \zeta_i \quad (9)$$

Here w is regarded as an optimization parameter, ζ_i is used as a slack variable, and C is called the penalty factor. With proper mapping through an appropriate kernel K , data that is difficult to be segregated in low-dimensional space can be made segregated in high-dimensional space, and classification decisions can be obtained as:

$$f(x) = \text{sign} \left(\sum_{i=1}^m \alpha_i y_i K(x, x_i) + b \right) \quad (10)$$

Here, α is the Lagrangian multiplier used for constrained optimization problem conversion to an unconstrained optimization problem. A quadratic kernel is adopted for high-dimensional mapping. Features are normalized in the range of 0–1, and five folds cross-validation is used to overcome over-fitting. The implementation is done in MATLAB 2022b environment using a workstation with 32 GB RAM and an i7-10510 U processor.

III. EXPERIMENTAL SETUP AND DATA ACQUISITION

A Machine Fault Simulator (MFS) is used for the experimental design as shown in Fig. 3. In general the peculiar features of a machine can have an impact on the diagnostic procedure. Also, the occurrence of faults in combination is a practical problem in

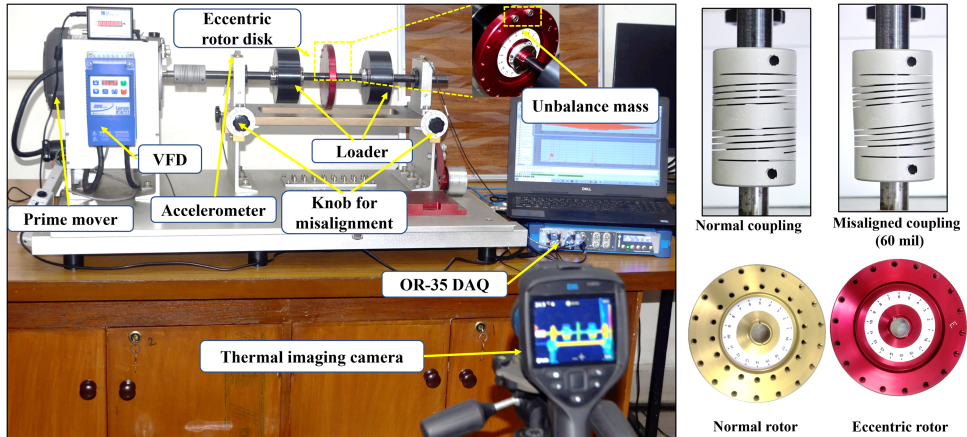


Fig. 3. Experimental setup and data acquisition of multi-sensor-based fault diagnosis.

TABLE I
ABBREVIATION OF FAULT CONDITIONS

Single faults		Dual faults		Multi-faults	
Condition	Label	Condition	Label	Condition	Label
U1	SF1	M1+U1	DF1	M1+U1+E	MF1
U2	SF2	M1+U2	DF2	M1+U1+U2+E	MF2
M1	SF3	M1+E	DF3	M2+U1+E	MF3
M2	SF4	M2+U1	DF4	M2+U1+U2+E	MF4
E	SF5	M2+U2	DF5		
		M2+E	DF6		
		U1+E	DF7		
		U2+E	DF8		

industrial machines. These are important concerns while doing the data acquisition of faults in a rotating mechanical system. MFS has the provision to experimentally simulate different combination of fault conditions that mimic the practical working conditions. In MFS, a squirrel cage induction motor is used as prime mover. The specifications of the motor are 3 phase, 2 pole, 440 V, 0.5 HP, and speed control is done by a variable frequency drive.

During the experimentation the prime mover is kept in healthy conditions. Different combinations of faults have been considered as dual and multi-faults. The healthy condition of rotating mechanical system is taken as baseline data and labeled as HL. In the present study, parallel misalignment of 30 mils (M1) and 60 mils (M2) are created. Similarly, unbalance of 6.12 gm (U1), and 12.24 gm (U2) are attached to the rotor disk. For the eccentricity fault (E), an eccentric rotor disk with an eccentricity of 2 mm is used, as shown in Fig. 3. The conditions and labels for single, dual, and multi-faults are given in Table I. Including HL, there are six classes for single fault conditions, nine for dual fault conditions, and five for multi-fault conditions. Fig. 4 is given with the principle of the three types of faults. Fig. 4(a) demonstrates the basic principle of parallel misalignment. When rotating machinery is having misalignment, reaction forces and moments are induced at the coupling (denoted by R and T respectively). These forces and moments cause the bending of elastomeric coupling and additional vibrations at the bearing, which become a potential source of heat generation at coupling and bearing housing locations. L shows the length of the coupling which is 70 mm. Fig. 4(b) shows the basic principle of unbalance.

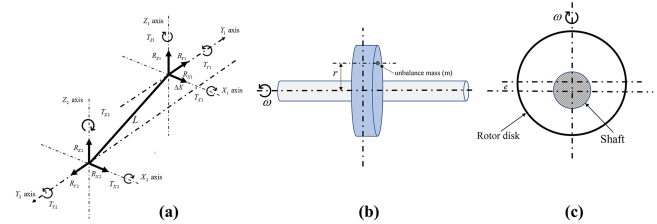


Fig. 4. Principle of investigated faults in the rotating mechanical system: (a) Parallel misalignment. (b) Unbalance. (c) Eccentricity.

Rotor unbalance is a frequent and significant cause of vibration in a rotating mechanical system that ultimately contributes to heat generation at the bearing regions. An unbalance force equivalent to $m\omega^2 r$ is induced. Here ω is the rotational speed, m is the unbalance mass located at radius r . Fig. 4(c) shows the eccentricity fault in the rotating mechanical system. The rotor center is offset by e from the center of shaft axis. Eccentricity mimics the unbalance and increases the radial vibrations that also cause heat generation at the bearing location.

For data acquisition, a FLIR-E95 IRT camera at a distance of 1 m is placed. The thermal sensitivity of the FLIR-E95 camera is 0.01°C i.e., it can sense minor differences in heat as small as 0.01°C at the target surface and display them as shades of different color palettes in the thermal image. IRT cameras are not only able to visualize thermal radiation, but this allows us to be aware of the presence of heat and evaluate its relative severity. The spectral range of the IRT camera is $7.5\text{ }\mu\text{m}$ – $14\text{ }\mu\text{m}$ with a resolution of 640×480 , and the frame rate is 23 frames/second. A uniaxial accelerometer (B&K-4533B001) is mounted at the drive end bearing housing location of the MFS as this location get affected most due to misalignment and unbalance [3]. It has a low-noise preamplifier with built-in Transducer Electronic Data Sheet (TEDS) functionality. The frequency range of this accelerometer is 0.2 Hz to 12.8 kHz with a resonance frequency of 35.4 kHz. The sensitivity of this accelerometer is 101.6 mV/g with an operating temperature range of -55°C to 125°C . The maximum non-destructive shock is 10000 g (peak). The sampling frequency for vibration data is taken as 6.4 kHz ensuring to eliminate the aliasing in the signal.

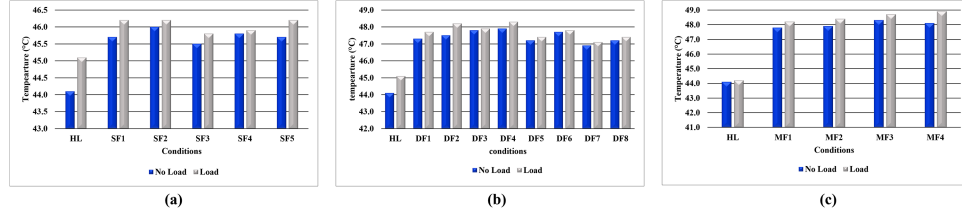


Fig. 5. Temperature on drive end bearing: (a) Single faults. (b) Dual faults. (c) Multi-faults.

TABLE II
DATA SIZE USED FOR TRAINING AND TESTING

Fault condition	Number of classes	Image samples in each class	Total samples
Single faults	6	6900	41400
Dual faults	9	6900	62100
Multi-faults	5	6900	34500

In the case of IRT camera, some critical parameters are emissivity, the distance between the target and camera, room temperature, and relative humidity. During the experimentation the room temperature was 26 °C and relative humidity was 40%. Among these factors, emissivity is taken as 0.9 according to housing material. The data is captured for the no-load and load conditions. For load conditions, loader of 5 kg is attached on both sides of the rotor at a distance of 10 cm. The speed is increased linearly up to 35 Hz in 1500 seconds to achieve steady state conditions as per the time constant of the simulator components [18]. For further stability and to achieve thermal equilibrium, the setup is run for another 300 seconds at 35 Hz. The data acquisition is then started for both IRT and vibration data for a period of 300 seconds. The recorded IRT video for this duration yields 6900 images after extraction for each class. The datasize of different fault conditions is given in Table II. Sufficient amount of data is an important concern for robust training of a model. The experimentation is done in an isolated chamber with insulated glass walls to bear the environmental effects of temperature variation to study the near to exact values of temperature in different fault conditions. There was no significant heat source inside the chamber that can hinder the results of IRT-based fault diagnosis.

IV. EXPERIMENTAL RESULTS AND DISCUSSION

The diagnosis performance based on IRT and vibration monitoring is analyzed in this section. The obtained results are analyzed in terms of confusion matrices and respective performance measures, including F1-score, specificity, and Matthews Correlation Coefficient (MCC). These parameters are calculated using the information from the confusion matrix (M) in terms of True Positives (TP_M), True Negatives (TN_M), False Positives (FP_M), and False Negatives (FN_M). The F1-score, which is expressed as the harmonic mean of precision (P_r) and recall (R_c), estimates the number of times a model accurately predicted the whole dataset [2]. The mathematical formulae of

F1-score is given as:

$$F1\text{-}score = \frac{2.P_r.R_c}{P_r + R_c} \quad (11)$$

$$\text{Here, } P_r = \frac{TP_M}{TP_M + FP_M}, \text{ and } R_c = \frac{TP_M}{TP_M + FN_M} \quad (12)$$

Another crucial performance metric, called specificity, concentrates on how accurately the classifier predicts fault states under pessimistic assumptions [13]. The specificity is given as:

$$\text{Specificity} = \frac{TN_M}{TN_M + FP_M} \quad (13)$$

Another trustworthy statistical metric is the MCC, which only yields a high score when the prediction performs well across the board for all four parameters of a confusion matrix [44]. MCC is given by the following expression shown at the bottom the next page.

A. IRT-Based Fault Diagnosis

IRT technology enables high-resolution and non-invasive observation of an object's surface temperatures. This makes it feasible to observe the temperature of rotating components during the machine run, such as bearing and coupling. Fig. 5 and Fig. 6 shows the temperature plots at different fault condition at the drive end bearing and coupling, respectively. It can be observed that in the case of single-faults, the discrimination of different conditions is apparent with significant clarity. From Fig. 5(a), it is evident that at unbalance conditions, the rise in temperature is higher than in other situations at no-load and load conditions. However, in the case of eccentricity fault, the temperature is more at load conditions rather than the no-load condition, which reflects the severity of this fault in load conditions and must be monitored to inhibit significant loss. Similarly, Fig. 5(b) and Fig. 5(c) show the temperature values for dual and multi-fault conditions, respectively.

Fig. 6 shows the temperature values in different fault conditions at the coupling. Fig. 6(a) shows that the effect of misalignment with 60 mil condition at coupling is significant compared to other fault conditions. Also, unbalance, and eccentricity fault conditions have lesser temperature values at coupling as compared to bearing location. Additionally, discriminating in cases of dual and multi-faults is generally better than in the preceding situation. Similarly, at coupling, the temperature values for the dual and multi-fault conditions are given in Fig. 6(b) and Fig. 6(c), respectively. Further, the discrimination of fault conditions only with temperature values is not always viable due to environmental constraints. In such cases, the pattern of

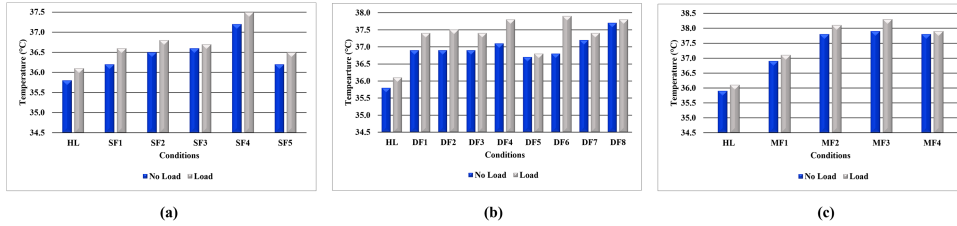


Fig. 6. Temperature on coupling: (a) Single faults. (b) Dual faults. (c) Multi-faults.

different fault conditions can be studied with pattern recognition at a steady state, as this condition is generally viable in industries, as discussed earlier. IRT provides a benefit for fault diagnosis as it is a non-invasive technique.

Fig. 7 shows the confusion matrices of single, dual, and multi-fault conditions at no-load. It is evident that all conditions are classified with 100% accuracy with no error. As discussed earlier, ROI includes both bearing and coupling for the extraction of features that helps to get the detailed information regarding the considered fault, i.e., misalignment, unbalance, and eccentricity, hence achieving perfect classification results. This facilitates to cover a broader span for inspection accurately and also in a fast manner as in industries machines run regularly. Similarly, Fig. 8 is given with the confusion matrices for load conditions using IRT. It is clear from Fig. 8(a) and Fig. 8(c) that the single and multi-faults conditions are perfectly classified, i.e., with 100% accuracy as well. However, there is a small error in classifying the condition of dual faults, as given in Fig. 8(b). DF1 and DF8 have an error of 0.1% in classification, and the same misclassification persisted among DF3 and DF4. As the classification accuracy of IRT is mostly found 100% or very close to it, the performance measures, including F1-score, specificity, and MCC, are also expected to reflect exemplary performance.

B. Vibration-Based Fault Diagnosis

Apart from having a fast, non-invasive, and covering broader area of diagnosis, IRT has some inherent issues. When individual objects have unpredictable temperatures, it might be challenging to interpret thermal images. So, it becomes necessary to use it in a complementary manner with established methods to form a multi-sensor system for a reliable fault diagnosis. Among these methods, vibration monitoring is proved to be the most reliable method for the identification of various faults. Single, dual, and multi-fault conditions are diagnosed in the same manner as applied for IRT. Here, CQT-based time-frequency images are used for feature extraction.

Fig. 9(a) shows the confusion matrix for the single fault condition at no-load using vibration data. It is evident that there is misclassification between healthy and low unbalance condition. The other conditions are classified with prevalently much better accuracy. However, it is evident from Fig. 9(b) and Fig. 9(c) that the performance classification is much better when it comes to the dual fault and multi-fault conditions, as the severity

TABLE III
COMPARISON OF THE PROPOSED METHOD WITH OTHER CLASSIFIERS

Fault Conditions	DCNN-Softmax		DCNN-kNN		DCNN-SVM	
	IRT	Vibration	IRT	Vibration	IRT	Vibration
Accuracy at No-Load (%)						
Single faults	100	89.49	100	92.3	100	92.4
Dual faults	100	98.69	100	99.3	100	99.4
Multi-faults	100	99.51	100	99.8	100	99.9
Accuracy at Load (%)						
Single faults	100	84.41	100	86.6	100	87.7
Dual faults	99.9	94.94	99.92	95.02	99.99	95.8
Multi-faults	100	96.8	100	97.9	100	98.1

inclusion increases the feature-based discrimination among the classes. Similarly, Fig. 10 shows the confusion matrices at load conditions in the case of vibration data. Fig 10(a) reflects that the misclassification is more among the two unbalance faults at the load condition as the unbalance mass gets suppressed due to load on both sides of the rotor. There is also slight misclassification between the two misaligned conditions for obvious reasons. However, the eccentric condition gets classified with the same 99.9% as it is there in the no-load conditions. Further, it is clear from Fig. 10(b) and Fig. 10(c) that the classification performance in the case of dual and multi-fault conditions is slightly lower at load condition than the no-load condition, with some misclassification among the classes. The performance measures based on vibration monitoring results are given in Fig. 11. It is evident from the figure that performance at no-load is better than the load condition. However, in the case of dual and multi-faults, the values of all three performance measures are more than 0.95.

C. Methodology Validation and Comparison With Reported Work

The performance of the proposed DCNN-SVM-based classification is also compared with two other prevalently used classifiers, including SoftMax and k-Nearest Neighbour (k-NN). Table III shows the performance of these classifiers against the proposed work. It shows that in all three sets of fault conditions, performance of all classifiers give 100% classification accuracy for IRT-based diagnosis except dual-faults at load conditions with slightly less accuracy than 100%. However, in the case of vibration monitoring, the proposed DCNN-SVM-based results are best among the considered classifiers that reflect the soundness of the suggested method.

$$\frac{(TP_M \cdot TN_M) - (FP_M \cdot FN_M)}{\sqrt{(TP_M + FP_M)(TP_M + FN_M)(TN_M + FP_M)(TN_M + FN_M)}} \quad (14)$$

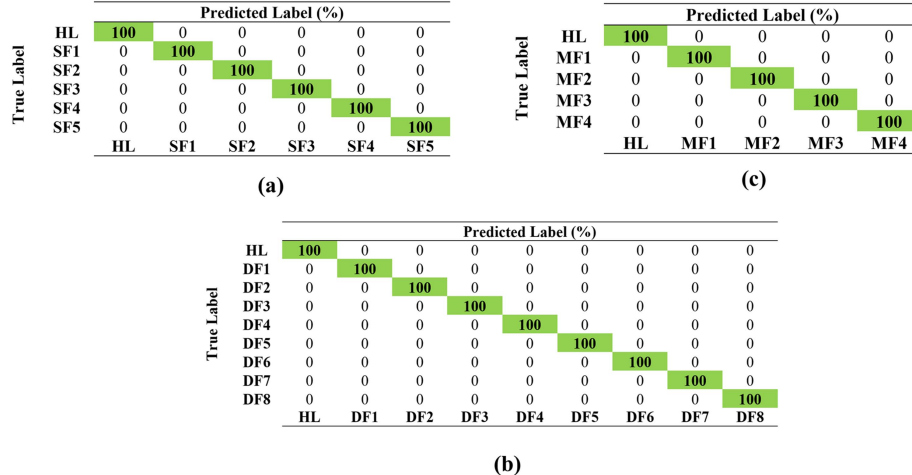


Fig. 7. IRT based results at no-load: (a) Single faults. (b) Dual faults. (c) Multi-faults.

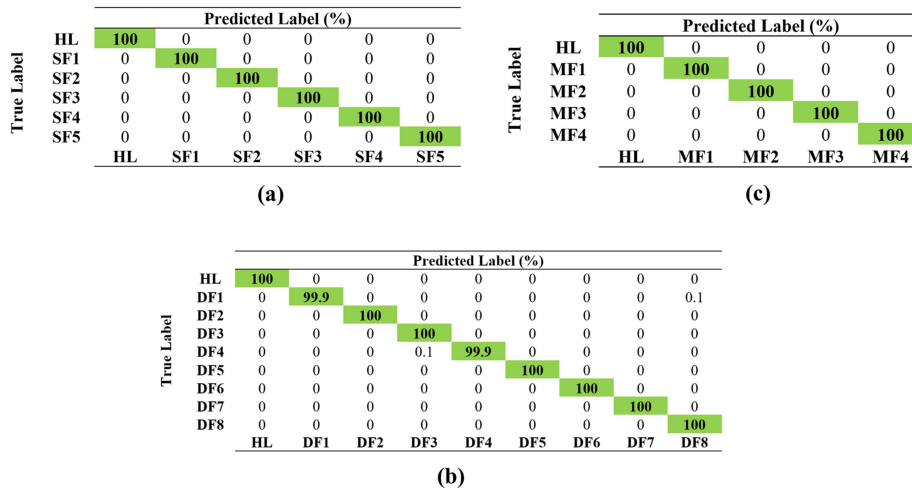


Fig. 8. IRT based results at load condition: (a) Single faults. (b) Dual faults. (c) Multi-faults.

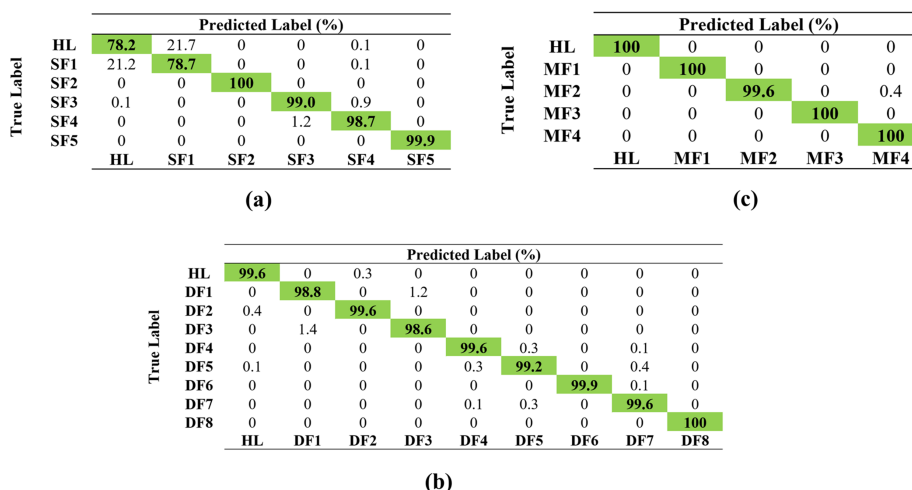


Fig. 9. Vibration monitoring based results at no-load: (a) Single faults. (b) Dual faults. (c) Multi-faults.

True Label	Predicted Label (%)					
	HL	SF1	SF2	SF3	SF4	SF5
HL	92.4	6.2	1.0	0.1	0.3	0
SF1	9.4	68.2	21.9	0.2	0.3	0
SF2	2.5	26.6	70.6	0.1	0.2	0
SF3	0.1	0.2	0	96.9	2.8	0
SF4	0.2	0.3	0.1	2.6	96.9	0
SF5	0	0	0.1	0	0	99.9
HL	99.9	0	0	0	0	0
MF1	0	97.1	1.0	1.3	0.5	
MF2	0	0.9	97.7	0	1.3	
MF3	0	1.2	0	98.1	0.7	
MF4	0	0.5	1.5	0.5	97.6	

True Label	Predicted Label (%)					
	HL	MF1	MF2	MF3	MF4	
HL	100	0	0	0	0	0
DF1	0	95.8	0.1	3.5	0.1	0.3
DF2	0	0	91.6	0	8.4	0
DF3	0	1.9	0	97.9	0	0.1
DF4	0	0	2.3	0	97.4	0.1
DF5	0	0	0.1	0	92.2	7.0
DF6	0	0.2	0	0.1	0.2	0.2
DF7	0	0.2	0	0.3	0	0.1
DF8	0	0.3	0.2	0	0	0.7
HL	DF1	DF2	DF3	DF4	DF5	DF6
					DF7	DF8

(a)

(c)

True Label	Predicted Label (%)							
	HL	DF1	DF2	DF3	DF4	DF5	DF6	DF7
HL	100	0	0	0	0	0	0	0
DF1	0	95.8	0.1	3.5	0.1	0.3	0.1	0
DF2	0	0	91.6	0	8.4	0	0	0
DF3	0	1.9	0	97.9	0	0	0.1	0.1
DF4	0	0	2.3	0	97.4	0.1	0.2	0
DF5	0	0	0.1	0	92.2	7.0	0.1	0.7
DF6	0	0.2	0	0.1	0.2	6.5	91.7	0.2
DF7	0	0.2	0	0.3	0	0.1	0.2	0.1
DF8	0	0.3	0.2	0	0	3.9	6.6	0.2
HL	DF1	DF2	DF3	DF4	DF5	DF6	DF7	DF8

(b)

Fig. 10. Vibration monitoring based results at load condition: (a) Single faults. (b) Dual faults. (c) Multi-faults.

TABLE IV
COMPARISON OF THE PROPOSED METHOD WITH REPORTED WORK

Reference	Modality	Fault condition	Fault combination	Feature extraction	Classifier	Maximum accuracy (%)
[45] (2021)	Vibration	Misalignment and unbalance	Single, and dual faults	Statistical features	SVM, kNN, and RF	97.92
[46] (2017)	Temperature	Misalignment	Single faults	-	-	-
[47] (2022)	Vibration and acoustic	Misalignment	Single faults	Statistical features	SVM	100.0
[48] (2021)	Speed	Misalignment	Single faults	Statistical features	SVM	100.0
Proposed	Infrared thermography and vibration	Misalignment, unbalance, eccentricity	Single, dual, and multi-faults	DCNN	SVM	100.0

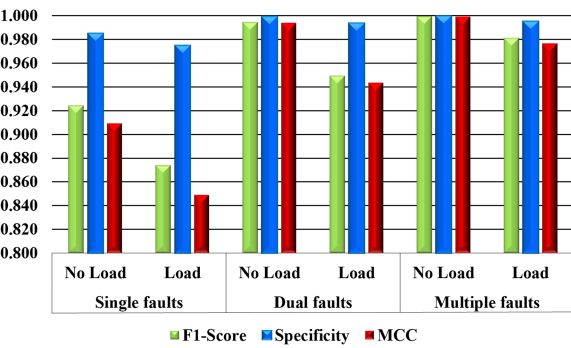


Fig. 11. Performance measures of vibration based results.

Further, the proposed work is also compared with the existing literature on misalignment and unbalance faults. In the literature, the work related to misalignment, unbalance, and eccentricity fault detection in rotating mechanical systems is majorly available using model-based approaches. These approaches are labor-intensive and less effective for the complex system. Some researchers have adopted data-driven approaches for the identification of these faults. A comparison of suggested method with some existing related work is discussed in Table IV based on used modality, fault condition, and fault combinations. Martins et al. [45] used vibration data to study different unbalance

and misalignment conditions and classified them using kNN, SVM, and RF. The best results were provided by SVM with an accuracy of 97.92%. Tonks et al. [46] presented a temperature monitoring system for different misalignment fault conditions in a rotating machine test rig. The results demonstrated the potential of temperature-based misalignment detection in rotating machines. A vibro-acoustic fusion-based strategy was presented by Patil et al. [47] for various misaligned conditions using SVM and observed prevalently good results for the diagnosis with 100% accuracy. Dias et al. [48] presented a fault diagnosis system for different misaligned conditions of the rotating machine using the data of speed from a cloud-based system. SVM was used for the classification of faults using various statistical features, and the maximum accuracy achieved was 100%. In these studies, the faults are primarily explored in single fault conditions, which is a nearly rare condition in the industry. In the proposed work, the combination of faults has been investigated using IRT and vibration monitoring to form a reliable fault diagnosis system. The results signify the performance of the proposed system.

D. Methodology Validation on Additional Dataset

The validation of the proposed methodology is experimentally done on different bearing fault conditions. The experiments are conducted on a bearing test rig, as shown in Fig. 12. A deep

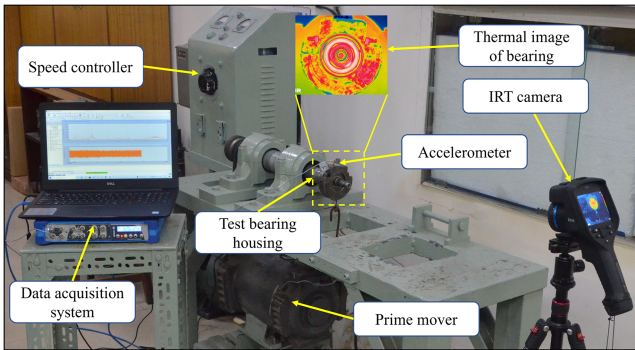


Fig. 12. Experiemental setup for bearing fault diagnosis.

		Predicted Label (%)				
		BHL	BIR	BOR	BBD	BLL
True Label	BHL	100	0	0	0	0
	BIR	0	100	0	0	0
True Label	BOR	0	0.1	100	0	0
	BBD	0	0	0	100	0
True Label	BLL	0	0	0	0	100
	BHL	100	0	0	0	0

		Predicted Label (%)				
		BHL	BIR	BOR	BBD	BLL
True Label	BHL	99.8	0	0.2	0	0
	BIR	0	100	0	0	0
True Label	BOR	0	0	100	0	0
	BBD	0	0	0	100	0
True Label	BLL	0	0	0	0	100
	BHL	99.8	0	0.2	0	0

Fig. 13. Results of bearing fault diagnosis based on: (a) IRT. (b) Vibration.

groove ball bearing (BB1B420205) is used for the study. The total number of balls in the bearing is 8, with each diameter of 8.7 mm. The inner and outer diameters are 25 mm and 52 mm, respectively. The pitch diameter of the bearing is 37.9 mm. The data for IRT and the vibration is acquired by varying the speed from 1140 rpm to 1740 rpm with a load of 10 kg.

The data acquisition is done for a total of 300 seconds. A DC motor of 2 HP is used as a prime mover to rotate the bearing test rig. The accelerometer is placed on the upper surface of the bearing housing, and the IRT camera is placed at a distance of 1 m from the bearing housing. The emissivity is taken as 0.55 as per the surface of the bearing housing. The room temperature and relative humidity during the experimentation were 30.3 °C and 28%, respectively. Four fault conditions are studied, including the healthy condition which is labeled as BHL. The faulty conditions include fault in the inner race (BIR), fault in the outer race (BOR), fault in the ball (BBD), and lack of lubrication (BLL). The BIR and BOR are created by making a through hole of 2 mm in the inner and outer race of the ball bearing using electric discharge machining. Similarly, the ball fault is created by rubbing one of the balls by 1 mm. For a healthy condition, 2.3 gm of grease is used as the manufacturer recommends. The lack of lubrication fault includes only 20% lubrication than the healthy condition. The results based on IRT and vibration are given in Fig. 13(a) and Fig. 13(b), respectively. It can be seen from these results that in the case of IRT, all the conditions are perfectly classified i.e., with 100% accuracy. Similarly, in the case of vibration-based results, only the healthy condition has a misclassification error of 0.2% with the outer race faults. Other conditions are classified with 100% accuracy, as shown in Fig. 13(b). These results with the proposed methodology on the additional dataset signify the applicability of the proposed methodology in industrial applications for the diagnosis of faults on rotating machines in different working environments.

V. CONCLUSION

The proposed work presented an intelligent multi-sensor fault diagnosis method using infrared thermography and vibration data. These modalities are used in a synchronized manner to resolve the issue related to the unmeasured state associated with commensurate modality sensors. The method is used for the diagnosis of frequently occurring faults in rotating mechanical system, including misalignment, unbalance, and rotor disk eccentricity as single, dual, and multi-faults. For an affordable, effective, and reliable system, a DCNN is utilized to extract image-based deep features along with PCA-based dimensionality reduction which is followed by SVM implementation for fault classification. The experimental findings revealed that detecting a different combination of faults is feasible if suitable pattern recognition is implemented. Additionally, with a maximum accuracy of 100%, the IRT-based technique outperformed the vibration monitoring based diagnosis in all three types of fault scenarios: single faults, dual faults, and multi-faults. These results demonstrate that the IRT can be used cogently and effectively with vibration monitoring to form a multi-sensor fault diagnosis system. As a prospective research, more complex fault conditions will be analyzed thoroughly using IRT and vibration monitoring based study in a synchronized manner.

REFERENCES

- [1] S. Pang, X. Yang, X. Zhang, and X. Lin, "Fault diagnosis of rotating machinery with ensemble kernel extreme learning machine based on fused multi-domain features," *ISA Trans.*, vol. 98, pp. 320–337, 2020.
- [2] L. C. Brito, G. A. Susto, J. N. Brito, and M. A. Duarte, "An explainable artificial intelligence approach for unsupervised fault detection and diagnosis in rotating machinery," *Mech. Syst. Signal Process.*, vol. 163, 2022, Art. no. 108105.
- [3] T. Mian, A. Choudhary, and S. Fatima, "Multi-sensor fault diagnosis for misalignment and unbalance detection using machine learning," in *Proc. IEEE Int. Conf. Power Electron., Smart Grid, Renewable Energy*, 2022, pp. 1–6.
- [4] Y. Xue, D. Dou, and J. Yang, "Multi-fault diagnosis of rotating machinery based on deep convolution neural network and support vector machine," *Meas.*, vol. 156, May 2020, Art. no. 107571.
- [5] J. Zhang, Q. Zhang, X. He, G. Sun, and D. Zhou, "Compound-fault diagnosis of rotating machinery: A fused imbalance learning method," *IEEE Trans. Control Syst. Technol.*, vol. 29, no. 4, pp. 1462–1474, Jul. 2021.
- [6] S. Prabhakar, A. S. Sekhar, and A. R. Mohanty, "Crack versus coupling misalignment in a transient rotor system," *J. Sound Vib.*, vol. 256, no. 4, pp. 773–786, 2002.
- [7] G. K. Yamamoto, C. da Costa, and J. S. da Silva Sousa, "A smart experimental setup for vibration measurement and imbalance fault detection in rotating machinery," *Case Stud. Mech. Syst. Signal Process.*, vol. 4, pp. 8–18 , 2016.
- [8] O. Janssens et al., "Convolutional neural network based fault detection for rotating machinery," *J. Sound Vib.*, vol. 377, pp. 331–345, Sep. 2016.
- [9] J. Piotrowski, *Shaft Alignment Handbook*. Boca Raton, FL, USA: CRC Press, 2007.
- [10] A. K. Jalan and A. Mohanty, "Model based fault diagnosis of a rotor-bearing system for misalignment and unbalance under steady-state condition," *J. Sound Vib.*, vol. 327, no. 35, pp. 604–622, Nov. 2009.
- [11] P. Kumar and R. Tiwari, "Finite element modelling analysis and identification using novel trial misalignment approach in an unbalanced and misaligned flexible rotor system levitated by active magnetic bearings," *Mech. Syst. Signal Process.*, vol. 152, 2021, Art. no. 107454.
- [12] A. R. Mohanty, *Machinery Condition Monitoring: Principles and Practices*. Boca Raton, FL, USA: CRC Press, 2014.
- [13] T. Mian, A. Choudhary, and S. Fatima, "An efficient diagnosis approach for bearing faults using sound quality metrics," *Appl. Acoust.*, vol. 195, 2022, Art. no. 108839.

- [14] A. Glowacz, "Fault diagnosis of electric impact drills using thermal imaging," *Meas.: J. Int. Meas. Confederation*, vol. 171, Feb. 2021, doi: [10.1016/j.measurement.2020.108815](https://doi.org/10.1016/j.measurement.2020.108815).
- [15] M. Delgado-Prieto, J. A. Carino-Corras, J. J. Saucedo-Dorantes, R. de Jesus Romero-Troncoso, and R. A. Osornio-Rios, "Thermography-based methodology for multifault diagnosis on kinematic chain," *IEEE Trans. Ind. Inform.*, vol. 14, no. 12, pp. 5553–5562, Dec. 2018.
- [16] R. A. Osornio-Rios, J. A. Antonino-Daviu, and R. de Jesus Romero-Troncoso, "Recent industrial applications of infrared thermography: A review," *IEEE Trans. Ind. Inform.*, vol. 15, no. 2, pp. 615–625, Feb. 2019.
- [17] T. A. Harris and M. N. Kotzalas, *Rolling Bearing Analysis*, vol. I. Boca Raton, FL, USA: CRC Press, 2007.
- [18] S. Fatima, A. R. Mohanty, and V. N. A. Naikan, "A misalignment detection methodology by measuring rate of temperature rise of shaft coupling using thermal imaging," *Proc. Inst. Mech. Eng. Part O J. Risk Rel.*, vol. 229, no. 3, pp. 209–229, 2015.
- [19] K. Y. Emre, N. Gürsel Ozmen, and L. Gümuşel, "Intelligent worm gearbox fault diagnosis under various working conditions using vibration sound and thermal features," *Appl. Acoust.*, vol. 186, 2022, Art. no. 108463.
- [20] G. Qian, S. Lu, D. Pan, H. Tang, Y. Liu, and Q. Wang, "Edge computing: A promising framework for real-time fault diagnosis and dynamic control of rotating machines using multi-sensor data," *IEEE Sensors J.*, vol. 19, no. 11, pp. 4211–4220, Jun. 2019.
- [21] H. B. Mitchell, *Multi-Sensor Data Fusion: An Introduction*. Berlin, Germany: Springer, 2007.
- [22] O. Janssens, M. Loccufier, and S. V. Hoecke, "Thermal imaging and vibration-based multisensor fault detection for rotating machinery," *IEEE Trans. Ind. Inform.*, vol. 15, no. 1, pp. 434–444, Jan. 2019.
- [23] M. L. Fung, M. Z. Q. Chen, and Y. H. Chen, "Sensor fusion: A review of methods and applications," in *Proc. IEEE 29th Chin. Control Decis. Conf.*, 2017, pp. 3853–3860, doi: [10.1109/CCDC.2017.7979175](https://doi.org/10.1109/CCDC.2017.7979175).
- [24] R. Liu, B. Yang, E. Zio, and X. Chen, "Artificial intelligence for fault diagnosis of rotating machinery: A review," *Mech. Syst. Signal Process.*, vol. 108, pp. 33–47, 2018.
- [25] Y. Lei, B. Yang, X. Jiang, F. Jia, N. Li, and A. K. Nandi, "Applications of machine learning to machine fault diagnosis: A review and roadmap," *Mech. Syst. Signal Process.*, vol. 138, 2020, Art. no. 106587.
- [26] H. Tang, Z. Liao, P. Chen, D. Zuo, and S. Yi, "A robust deep learning network for low-speed machinery fault diagnosis based on multikernel and RPCA," *IEEE/ASME Trans. Mechatronics*, vol. 27, no. 3, pp. 1522–1532, Jun. 2022.
- [27] S. Tang, S. Yuan, and Y. Zhu, "Deep learning-based intelligent fault diagnosis methods toward rotating machinery," *IEEE Access*, vol. 8, pp. 9335–9346, 2020.
- [28] Q. Hu, A. Qin, Q. Zhang, J. He, and G. Sun, "Fault diagnosis based on weighted extreme learning machine with wavelet packet decomposition and KPCA," *IEEE Sensors J.*, vol. 18, no. 20, pp. 8472–8483, Oct. 2018.
- [29] J. Takabi and M. M. Khonsari, "Experimental testing and thermal analysis of ball bearings," *Tribol. Int.*, vol. 60, pp. 93–103, Apr. 2013.
- [30] K. Prabith and I. R. P. Krishna, "The numerical modeling of rotor-stator rubbing in rotating machinery: A comprehensive review," *Nonlinear Dyn.*, vol. 101, no. 2, pp. 1317–1363, 2020.
- [31] L.-C. Thomas, *Fundamentals of Heat Transfer*. Englewood Cliffs, NJ, USA: Prentice-Hall, 1980.
- [32] G. Meneghetti, "Analysis of the fatigue strength of a stainless steel based on the energy dissipation," *Int. J. Fatigue*, vol. 29, no. 1, pp. 81–94, 2007.
- [33] W. Li, Z. Cui, M. Jin, S. Yu, and X. Wang, "Dynamic temperature measurement with a dual-thermocouple sensor based on a dual-head one-dimensional convolutional neural network," *Measurement*, vol. 182, Sep. 2021, Art. no. 109679.
- [34] Y. Liu, C. Miao, X. Li, J. Ji, and D. Meng, "Research on the fault analysis method of belt conveyor idlers based on sound and thermal infrared image features," *Meas. J. Int. Meas. Confed.*, vol. 186, 2021, Art. no. 110177.
- [35] T. Mian, A. Choudhary, and S. Fatima, "Vibration and infrared thermography based multiple fault diagnosis of bearing using deep learning," *Nondestruct. Test. Eval.*, vol. 38, no. 2, pp. 275–296, 2022.
- [36] M. T. Pham, J.-M. Kim, and C. H. Kim, "Rolling bearing fault diagnosis based on improved GAN and 2-D representation of acoustic emission signals," *IEEE Access*, vol. 10, pp. 78056–78069, 2022.
- [37] N. Holighaus, M. Döfler, G. A. Velasco, and T. Grill, "A framework for invertible, real-time constant-Q transforms," *IEEE Trans. Audio, Speech, Lang. Process.*, vol. 21, no. 4, pp. 775–785, Apr. 2013.
- [38] J. Miao, J. Wang, and Q. Miao, "An enhanced multifeature fusion method for rotating component fault diagnosis in different working conditions," *IEEE Trans. Rel.*, vol. 70, no. 4, pp. 1611–1620, Dec. 2021.
- [39] Q. Song, M. Wang, W. Lai, and S. Zhao, "On Bayesian optimization-based residual CNN for estimation of inter-turn short circuit fault in PMSM," *IEEE Trans. Power Electron.*, vol. 38, no. 2, pp. 2456–2468, Feb. 2023.
- [40] T. He, Y. Liu, Y. Yu, Q. Zhao, and Z. Hu, "Application of deep convolutional neural network on feature extraction and detection of wood defects," *Measurement*, vol. 152, 2020, Art. no. 107357.
- [41] D. Zhang, Y. Chen, F. Guo, H. R. Karimi, H. Dong, and Q. Xuan, "A new interpretable learning method for fault diagnosis of rolling bearings," *IEEE Trans. Instrum. Meas.*, vol. 70, pp. 1–10, 2021.
- [42] A. A. Mohammed, R. Minhas, Q. M. J. Wu, and M. A. Sid-Ahmed, "Human face recognition based on multidimensional PCA and extreme learning machine," *Pattern Recognit.*, vol. 44, no. 10, pp. 2588–2597, 2011.
- [43] J. S. L. Senanayaka, H. V. Khang, and K. G. Robbersmyr, "Toward self-supervised feature learning for online diagnosis of multiple faults in electric powertrains," *IEEE Trans. Ind. Inform.*, vol. 17, no. 6, pp. 3772–3781, Jun. 2021.
- [44] R. Tong, P. Li, L. Gao, X. Lang, A. Miao, and X. Shen, "A novel ellipsoidal semisupervised extreme learning machine algorithm and its application in wind turbine blade icing fault detection," *IEEE Trans. Instrum. Meas.*, vol. 71, pp. 1–16, 2022.
- [45] D. S. S. Martins et al., "Diagnostic and severity analysis of combined failures composed by imbalance and misalignment in rotating machines," *Int. J. Adv. Manuf. Technol.*, vol. 114, pp. 3077–3092, 2021.
- [46] O. Tonks and Q. Wang, "The detection of wind turbine shaft misalignment using temperature monitoring," *CIRP J. Manuf. Sci. Technol.*, vol. 17, pp. 71–79, May 2017.
- [47] S. Patil, A. K. Jalan, and A. M. Marathe, "Support vector machine for misalignment fault classification under different loading conditions using vibro-acoustic sensor data fusion," *Exp. Tech.*, vol. 46, no. 6, pp. 957–971, 2022.
- [48] A. L. Dias, A. C. Turcato, G. S. Sestito, D. Brandao, and R. Nicoletti, "A cloud-based condition monitoring system for fault detection in rotating machines using PROFINET process data," *Comput. Ind.*, vol. 126, 2021, Art. no. 103394.



Tauheed Mian received the B.E. and M.Tech. degrees from Aligarh Muslim University, Aligarh, India, in 2016 and 2018, respectively. He is currently a Ph.D. Student with the Centre for Automotive Research and Tribology, Indian Institute of Technology Delhi, New Delhi, India. His research interest includes fault diagnosis and prognosis of rotating machines, applied artificial intelligence, industrial IoT, machinery NVH, EV diagnostics, and manufacturing systems.



Anurag Choudhary (Member, IEEE) received the B.Tech. degree in electrical and electronics engineering from Uttarakhand Technical University, Dehradun, India and the M.E. degree in instrumentation and control from Panjab University, Chandigarh, India. He is currently a Ph.D. Student with the School of Interdisciplinary Research, Indian Institute of Technology Delhi, New Delhi, India. He has authored or coauthored more than 20 papers in various reputed journals. His research interests include fault diagnosis, vibration monitoring, infrared thermography, electric vehicles, and applied artificial intelligence.



Shahab Fatima received the M.S. and Ph.D. degrees from the Indian Institute of Technology Kharagpur, Kharagpur, India, in 2011 and 2014, respectively. She is currently an Associate Professor with the Centre for Automotive Research and Tribology, Indian Institute of Technology Delhi, New Delhi, India. She has authored or coauthored more than 30 papers in various reputed journals. Her research interests include machinery health monitoring, NVH, machinery and industrial noise control, and automotive health monitoring.